Sulaimani Journal for Pure and Applied Sciences Vol. 28 Issue 1 (2026) 75-95.

Journal homepage https://sjpas.univsul.edu.iq

Sulaimani Journal for Pure and Applied Sciences

ISSN:1812-4100

Original Article

Green Synthesis of Silver Nanoparticles Using Hellenocarum amplifolium Leaf Extract and Evaluation of Their Antibacterial and Antibiofilm Activities Against Some Uropathogens

Karzan Gh. Karim[a], Dana Khdr Sabir[b*] and Pshtiwan S. A Bebane[a]

[a] Department of Medical Laboratory Analysis, College of Science, Charmo University, 46023 Chamchamal, Kurdistan Region, Iraq.

[b] Department of Pharmaceutical Chemistry, College of Science, Charmo University, 46023 Chamchamal, Kurdistan Region, Iraq.

ARTICLE INFO

Article History:
Received: 28/02/2026
Revised: 19/03/2026
Accepted: 25/03/2026
Published online: 25/6/2026

Key Words:
Urinary tract infections
Hellenocarum amplifolium
Biosynthesis
Silver nanoparticles
Antibacterial
Antibiofilm

ABSTRACT

Urinary tract infections (UTIs) are among the most common bacterial infections worldwide, affecting millions of individuals each year. Their treatment has become more difficult as a result of the increasing prevalence of multidrug-resistant (MDR) pathogens. Although plant-mediated silver nanoparticles (AgNPs) have attracted considerable attention as alternative antibacterial drugs, their antibiofilm activity against bacteria isolated from UTI patients, remains insufficiently explored. In this study, AgNPs were biosynthesized using the aqueous leaf extract of the local Kurdistan plant *Hellenocarum amplifolium*, which acted as both a reducing and stabilising agent, and their antibacterial and antibiofilm activities were assessed against bacteria isolated from UTI patients. Bacterial isolates were initially identified with the VITEK® 2 Compact system and validated by 16S rRNA gene sequencing; these include *Acinetobacter baumannii*, *Escherichia coli*, *Staphylococcus haemolyticus*, and *Staphylococcus aureus*. The biofabricated *Hellenocarum amplifolium*- silver nanoparticles (Ha-AgNPs) were characterised by UV–Vis, FTIR, SEM, HR-TEM, XRD, and EDS analyses, revealing crystalline, nearly spherical nanoparticles with an average size of approximately 20 nm. Antimicrobial efficacy assessed by MIC and MBC assays demonstrated strong inhibitory effects at 25/50 µg/mL against *A. baumannii* and 50/75 µg/mL against *E. coli*, *S. haemolyticus*, and *S. aureus*. In addition, Ha-AgNPs exhibited pronounced antibiofilm activity against all tested isolates, with concentration-dependent inhibition reaching up to 97–99%. Overall, this study demonstrates the potential of Ha-AgNPs produced from *H. amplifolium* as potent antibacterial and antibiofilm agents, and presents an eco-friendly method of Ha-AgNP synthesis. These findings offer a promising alternative strategy to address antibiotic-resistance, although further studies are needed to assess its reliability and applicability in clinical settings.

OPEN ACCESS

1. Introduction

Urinary tract infections (UTIs) are among the most prevalent bacterial diseases in the world, affecting nearly 150 million individuals each year and substantially raising morbidity and death throughout the world (Diksha et al., 2023). Although both genders can get UTIs, it occurs more frequently in females, with 50% of women experiencing at least one infection during their lifetime, recurrence is also

* Corresponding author.
E-mail address: dana.sabir@chu.edu.iq (D. Sabir)

common. Female anatomy, sexual behavior, as well as family history are risk factors (Faruk et al., 2023). Both kidney (pyelonephritis) and bladder (cystitis) infections are possible (Timm et al., 2025). While many organisms can cause UTIs, common causative agents include Staphylococcus aureus, Candida albicans, Acinetobacter baumannii, Pseudomonas aeruginosa, Staphylococcus haemolyticus, Escherichia coli, Klebsiella pneumonia and Proteus mirabilis (Singh and Agri, 2024; Taha, 2024). A major worldwide healthcare concern is the rapid development of resistance in both Gram-positive (GP) and Gram-negative (GN) bacteria due to the widespread abuse and overuse of antibiotics (Divya et al., 2019).

Antimicrobial resistance has grown into an important global health issue in recent years and has become increasingly concerning, according to the World Health Organization (Abadi et al., 2019). Antibiotic-resistant bacteria have become a major issue in modern society, leading to the rise of superbugs (Shriram et al., 2018). A particular concern in developing countries is the increase in drug-resistant urinary tract infection (UTI) pathogens (Sher et al., 2024). Nitrofurantoin, fosfomycin, fluoroquinolones, cefpodoxime, and amoxicillin-clavulanic acid are all antibiotics that are often utilised for treating UTIs (Al Lawati et al., 2024). Because of the broad and inappropriate usage of antibiotics for UTI treatment, the uropathogens become multidrug-resistant, which increases the morbidity and mortality rates (Diksha et al., 2023). The failure of most antibiotics, besides the side effects, necessitates the search for better treatment options. Therefore, there is a need for alternative therapeutic options against antimicrobial-resistant bacteria (Mohanta et al., 2020).

In the last several years, the field of nanotechnology has made substantial improvements, resulting in the creation of nanoparticles with dimensions spanning from 1 to 100 nm. These particles possess distinctive physicochemical properties that are not present in bulk materials (Joseph et al., 2023). Among these, metal nanoparticles synthesized through biological routes have attracted a significant interest for medical applications because of their effectiveness and environmental sustainability (Abbasi et al., 2023). Silver nanoparticles (AgNPs), in particular, are widely investigated in nanomedicine due to their strong and broad-ranging antibacterial capacity as well as low cellular toxicity (Ahmed et al., 2018; Ali et al., 2024). Physical, chemical, or biological methods can be employed to synthesise AgNPs, but plant-mediated biosynthesis is regarded as eco-friendly, economical and efficient due to the phytoconstituents serving as stabilising and reducing agents in plant extracts (Nemma and Sadeq, 2023).

Despite extensive reports on green-synthesized AgNPs, studies employing clinically confirmed MDR uropathogens and systematic antibiofilm evaluation remain limited. Hellenocarum amplifolium, also known locally as Baraza, is an edible herb with traditional therapeutic uses such as diuretics and kidney stone treatment (Ahmad and Askari, 2015; Pieroni et al., 2017) ; however, its application in Ha-AgNP biosynthesis and antibiofilm assessment against clinical UTI isolates has not yet been explored.

H. amplifolium is a flowering plant in the Apiaceae family, known for aromatic herbs with umbels and a long history of use in both food and traditional medicine. This genus is native to southeastern Europe and the broader Mediterranean region, while H. amplifolium also grows wild in the rocky and mountainous areas of Iraq and neighboring regions (Zakharova et al., 2016; Qalatopzany et al., 2025). Locally, its young leaves are consumed as a vegetable and employed to treat digestive issues and mild infections. Phytochemical studies reveal that H. amplifolium is rich in phenolics, flavonoids, and volatile compounds such as linalool and limonene, which underlie its antioxidant and antimicrobial properties and make it an excellent candidate for the green synthesis of silver nanoparticles (Qalatopzany et al., 2025).

This research aims to biosynthesize and characterize Ha-AgNPs using H. amplifolium leaves aqueous extract and evaluate their antibacterial/antibiofilm effects against clinically isolated S. haemolyticus, E. coli, S. aureus, and A. baumannii from UTI patients in Chamchamal, Sulaymaniyah, Iraq.

2. Materials and Methods

2.1. Bacteria Strain Isolation and Identification

Bacterial isolates used in this study were initially isolated from urine samples of patients diagnosed with urinary tract infections (UTIs) and were kindly provided by the staff of Chamchamal Central Laboratory. The isolates were collected in November 2024 and were primarily identified using the VITEK® 2 Compact system. A single colony from each isolate was cultured in nutrient broth, and aliquots of the cultures were preserved as glycerol stocks and stored at −20 °C for subsequent analyses. Molecular identification was performed based on 16S rRNA gene sequencing. according to a previously described PCR procedure (Mohamedsalih and Sabir, 2020). Genomic DNA was extracted from the bacterial isolates using the Presto™ Mini gDNA Bacteria Kit (Geneaid, Taiwan) according to the manufacturer's instructions. PCR was performed in a total reaction volume of 20 µL, containing 10 µL of master mix, 1.5 µL of forward primer, 1.5 µL of reverse primer, 1 µL of DNA template, and 6 µL of ddH_2O. The 16S rRNA gene was amplified using universal primers: forward primer 5′-AGAGTTTGATYMTGGCTCAG-3′ and reverse primer 5′-ACGGYTACCTTGTTACGACTT-3′ (Satokari et al., 2001; Mohamedsalih and Sabir, 2020). The PCR technique begins with denaturation at 95°C (5 minutes), then continues with 36 cycles of denaturing at 95°C (30 seconds), annealing at 58°C (30 sec), and elongation at 72°C (2 min). The last elongation lasted 5 minutes at 72°C. Sanger DNA sequencing was used to purify and sequence the PCR products at Macrogen's Republic of Korea. The sequences were analyzed and assembled using the Chromas program version 2.0.

2.2. Phylogenetic Tree Construction

The isolates were taxonomically defined by constructing a phylogenetic sketch based on its previously reported 16S rRNA gene sequence (Chong et al., 2014). Using the NCBI WebSub, partial 16S rRNA gene sequences from the clinical isolates were submitted to GenBank to receive accession numbers (accession number). ClustalX2.1 was used to compare the clinical isolate's 16S rRNA sequences with those of closely related species to identify it at the taxonomic level (Larkin et al., 2007). MEGA 7 program was then used to evaluate the aligned sequences (Kumar et al., 2016). MEGA-7 program was employed to create a phylogenetic sketch utilizing the neighbor-joining approach, which was supported by 1000 bootstrap repetitions.

2.3. Collecting and Preparing H. amplifolium Leaf Extract

Leaves taken from the *H. amplifolium* plant were utilized to create Ha-AgNPs following a previously published procedure (Ali et al., 2024). In summary, fresh leaves of *H. amplifolium* leaves as seen in (Figure 1.b) were harvested from Suren Mountain (35°43'26"N, 46° 0' 0"E; Figure 1.a), Said Sadiq, Kurdistan Region, Iraq, in March 2024. The plant was later identified by experts at the College of Agricultural Engineering Sciences at the University of Sulaimani in Iraq, and the voucher sample was deposited (Voucher No. 5052). After the tap water was used to wash and remove debris and other organic contaminants from the leaves, and then the leaves of the plant were cleaned, and shade-dried, the leaves were ground with a blender until a powdered form, and kept in an airtight container for further use. To make the aqueous extract of *H. amplifolium leaves*, 10 g of dried leaves powder were put in a 600 ml container (beaker) with 200 ml of water that had been deionized. To extract compounds, the mixture was heated to 40 °C and stirred for two hours. After extraction, all insoluble plant debris was removed from the aqueous extract of the leaves by passing it through Whatman filter paper (Grade No. 1), then centrifuged the filtered extract at 6000 RPM for 25

minutes to remove any remaining particles or impurities. Finally, the purified extract was collected in a 50 mL bottle (falcon tube) and kept them at 4°C for further examination or testing.

2.4. AgNPs Synthesis from H. amplifolium Leaves Extract

AgNPs were prepared by H. amplifolium leaves extract and a silver nitrate salt. A 1 mM silver nitrate solution was prepared by dissolving the required amount (0.017 g) of salt in 100 mL of distilled H_2O. Then, 100 mL of the H. amplifolium leaves aqueous (water) extract was mixed with 100 mL of silver nitrate solution (1:1, v/v) to make a mixture at 60 ±2 °C using a hot plate for two hours while being constantly stirred, the pH of the mixture was 7.13, and it was kept in dark conditions by wrapping aluminium foil around the beaker during the reaction. The phytochemical constituents in H. amplifolium extract reduce Ag^+ ions into metallic Ag^0 nanoparticles during nucleation and also stabilise and cap nanoparticles to prevent aggregation. The solution's colour turned from colourless to light-brown when Ha-AgNPs were formed, as shown in (Figure 2) (Aslam et al., 2021). For purification, the solution containing Ha-AgNPs was centrifuged at 6000 rpm for 30 minutes, after which the supernatant was thrown out. After being rinsed with DDH2O, the precipitate was centrifuged at 10,000 rpm for 20 minutes to filter out any unreacted extract. The end product was oven dried at 45-50°C and preserved in a dark place for either further analysis (Aisida et al., 2019).

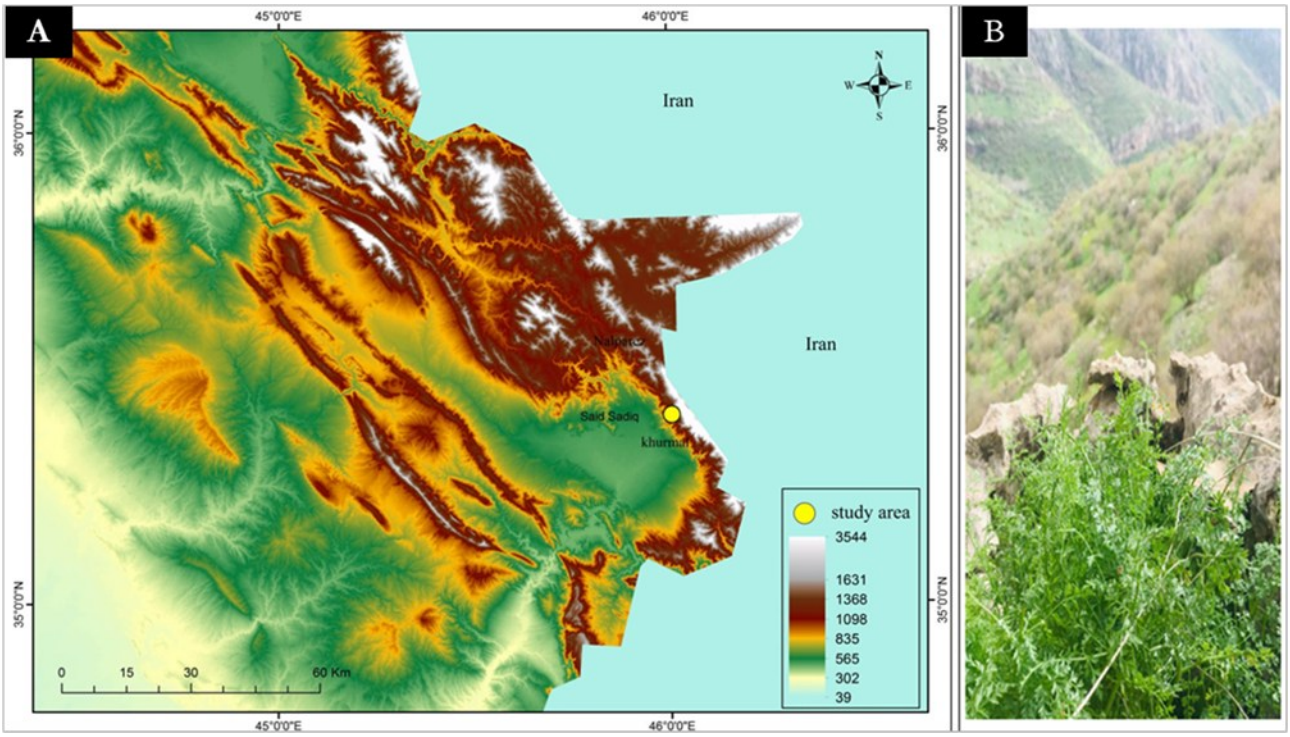

Figure 1. (A): Collection site of H. amplifolium at Suren Mountain, close to Said Sadiq, Al Sulaymaniah in the Kurdistan Region of Iraq. The yellow marker indicates the sampling site (35°43'26"N, 46° 0' 0"E). Meters are used to display elevation. (B): leaves of the H. amplifolium plant.

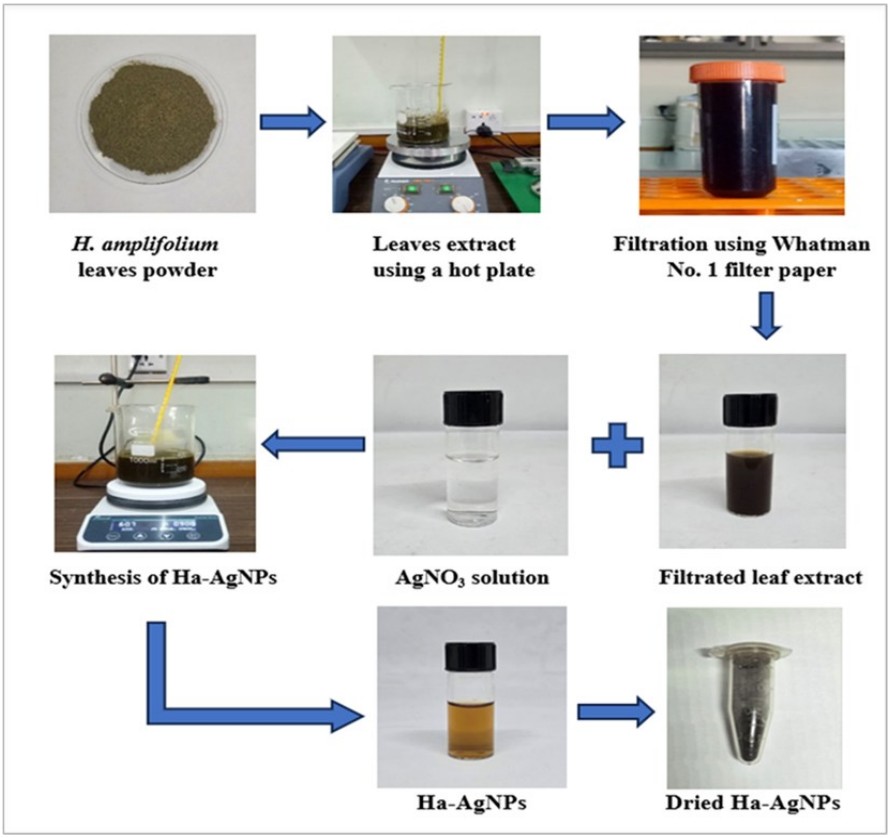

Figure 2. Biosynthesis of Ha-AgNPs by H. amplifolium leaf extract. Leaf powder was extracted and filtered, after being mixed with $AgNO_3$ solution for biofabricated of Ha-AgNPs. The Ha-AgNPs were collected and dried for further test.

2.5. Characterizing Biosynthesized H. amplifolium AgNPs

The following techniques were employed to characterize the fabricated Ha-AgNPs:

2.5.1. UV-visible Spectrophotometer

The UV-Vis adsorption spectrum of the synthesized Ha-AgNPs were investigated by a SI Analytics UV Line 9400 (Dublin, Germany) with scanning range of measurement wavelengths from between (200-800) nm. For this, 3 mL of Ha-AgNPs solution was introduced in the UV-Vis cuvette.

2.5.2. Analysis of FTIR

The different Functional groups of *H. amplifolium* leaf extract and synthesized Ha-AgNPs were identified using a Shimadzu FT-IR spectrometer. The process involved creating a final pellet by mixing the dried AgNPs with potassium bromide (KBr), and the mixture was then processed using FTIR spectroscopy in the 4000-400 cm-1 range.

2.5.3. Analysis of XRD

To assess the crystal structure and particle size of the fabricated Ha-AgNPs. For XRD analysis, the PanAnalytical X "Pert Pro diffractometer" (Almelo, The Netherlands) has been used at 45 kV and 40 mA, respectively. The range of the XRD glancing angles was $10° \leq 2\theta \leq 80°$. The sample was used for this test after it had been dried and converted into a powder. Based on XRD data, the Debye-Scherrer equation determined Ag-NP crystallite size.

$$\text{Crystalize Size } D \text{ (nm)} = \frac{K\lambda}{\beta cos\theta}$$

D: average particle size (nm), K: shape factor (0.90), λ: X-ray wavelength (0.15406), β: FWHM of the most extreme peak, θ: Bragg angle.

2.5.4. Analysis of Scanning Electron Microscopy (SEM)

The surface shape and size of the biofabricated silver nanoparticles were investigated by SEM. Nanoparticle samples were air-dried and deposited as a thin film on a suitable holder for final measurements. SEM images were taken with a CamScan 3200 LV microscopy (Caesium™ version 6.1).

2.5.5. Energy-Dispersive X-ray Spectroscopy (EDS) analysis

The EDS spectrum of the prepared Ha-AgNPs was recorded by using a JEOL JSM-7610F scanning electron microscope from (JEOL, Japan) to determine the elemental composition. EDS spectra were utilized to confirm presence of silver (Ag) and determine other related elements.

2.5.6. Analysis of High Resolution Transmission Electron Microscopy (HR-TEM)

The size and surface shape of Ha-AgNPs were studied using HR-TEM (Thermo Fisher Scientific, Germany). One drop of the Ha-AgNPs solution that had been prepared was deposited on copper grids that had been coated with carbon. Subsequently, the water was vaporised naturally at ambient temperature to form a sample. The TEM micrographs were then examined to investigate the distribution of particle sizes of produced Ha-AgNPs. HR-TEM images were used to confirm the crystalline structure.

2.6. Antibacterial Activity Assays of Ha-AgNPs

Using minimum inhibitory concentration (MIC) and minimum bactericidal concentration (MBC) tests, the antibacterial efficacy of Ha-AgNPs against clinically isolated bacterial strains was assessed. A Ha-AgNP stock solution (100 µg/mL) was prepared by dispersing 0.001 g of nanoparticles in 10 mL of sterile distilled-water and sonicating for 10–15 min; the suspension was stored at 3-4 °C until use. MIC values were determined by broth microdilution in sterile 96-well round-bottom. Clinical isolates of *E. coli*, *S. aureus*, *S. haemolyticus* and *A. baumannii* were cultivated in LB broth at 37 °C for 20-24 h, adjusted to 1×10^8 CFU/mL (0.5McFarland), and 120 µL of each suspension was inoculated per well. Ha-AgNPs were added (80 µL per well) to obtain final concentrations of 6.25, 12.5, 25, 50, 75, and 100 µg/mL. Wells containing bacterial suspension with LB broth and LB broth alone served as positive and negative controls, respectively. Plates were incubated at 37 °C for 22-24 h with shaking, and bacterial growth was assessed by measuring absorbance at 600 nm using microplate reader (Bio-Tech, USA). 5 µL aliquots from all wells that exhibit visible or not visible growth were spot-plated onto nutrient agar and incubated at 37 °C for 22–24 hours to determine MBC level. The MBC was determined to be the lowest Ha-AgNP concentration that did not exhibit bacterial regrowth (Fattah et al., 2022).

2.7. Antibiofilm Activity of Ha-AgNPs

The antibiofilm activity of Ha-AgNPs against *A. baumannii*, *E. coli*, *S. haemolyticus*, and *S. aureus* was determined using 96-well microtiter plates (polystyrene flat-bottom microwell plates). Bacterial strains were grown as previously described and adjusted to 1×10^8 CFU/mL (0.5 McFarland). Bacterial suspensions (120 µL) were inoculated into sterile flat-bottomed polystyrene 96-well, followed by the addition of 80 µL of Ha-AgNPs at different concentrations (1/2, 1/4, 1/8, 1/16, 1/32, and 1/64 MIC) using the sub-minimum inhibitory concentrations (sub-MICs) method (Swidan et al., 2022). Positive control wells contained bacterial culture with LB broth, while negative controls contained only LB broth. Plates were incubated at 37°C for 22-24 hours to promote the growth of biofilms.

Following incubation, non-adherent cells were washed away by phosphate-buffered saline (pH 7.2) three times and the plates were air dried. The adherent biofilm was then stained with 0.1% crystal violet for 20-25 min, washed by DDH2O to remove any unbound dye and air dried for about an hour; the bound crystal violet was dissolved in 96% ethanol (200 µL) and left in each well for 15-20 min

(Fattah et al., 2022; Fattah et al., 2026). Absorbance was measured at 595 nm using a microplate (BioTech/USA) reader to assess biofilm biomass.

The percentage of biofilm inhibition was estimated using the following formula (Kalishwaralal et al., 2010; Hasan et al., 2014).

$$\text{Biofilm inhibition (\%)} = \left(1 - \frac{\text{OD595}\textit{treated} \text{ with Ag} - \text{NPs}}{\text{OD595}\textit{control}}\right) \times 100$$

2.8. Statistical Analysis

GraphPad Software Inc.'s Prism 10 (One-Way ANOVA) was used for statistical analysis. The results of each experiment were recorded in triplicate and are presented as the mean ± standard deviation. Differences between control and treatment groups were analyzed to evaluate their significance. A p-value < 0.05 indicated significance.

3. Results and Discussion

The increasing prevalence of MDR bacteria, particularly in UTIs, has reduced the effectiveness of conventional antibiotics and underscores the need for alternative antimicrobial strategies. AgNPs have attracted considerable interest for their wide-spectrum antibacterial activity and high efficacy at low concentrations (Pachaiappan et al., 2021; Said et al., 2024), which are significantly impacted by the synthesis route, shape, and particle size (Slavin et al., 2017). Plant-mediated biosynthesis provides a low-cost, environmentally favourable, safe approach, with plant secondary metabolites acting as natural reducing and stabilizing agents (Said et al., 2024). *H. amplifolium* (Baraza), a medicinal plant that is extensively employed in the Kurdistan region of Iraq, represents a promising source of bioactive compounds (Ahmad and Askari, 2015; Pieroni et al., 2017). In this study, Ha-AgNPs biosynthesized using *H. amplifolium* leaf extract were tested for their antibacterial and antibiofilm activity against MDR bacteria.

3.1. Isolation and Identification of Bacteria Strains

The bacteria isolates were first identified with the VITEK® 2 Compact system (Figure 1 supplement) and then confirmed by 16S rRNA gene sequencing. Both 16S rRNA homology sequence searching and the phylogenetic tree analysis revealed that the bacteria are *A. baumannii*, *E. coli*, *S. haemolyticus*, and *S. aureus* and the four isolates' phylogenetic tree analysis showed they are related to closely related species in the database (Figure 3). The nucleotide 16S rRNA gene sequences were submitted to the NCBI WebSub along with their accession number: *A. baumannii* strain charmoK (PQ967975.1), *E. coli* strain charmoE (PQ967976.1), *S. haemolyticus* strain charmoH (PQ967977.1), and *S. aureus* strain charmoS (PQ967978.1).

As shown in Figure 3, the newly isolated *E. coli* strain charmoE, for instance, forms a monophyletic group with other *E. coli* strains, including strain SK-28 (accession number: PQ001789.1), which was isolated from Pakistan; strain EC103E (accession number: MT453878.1), which was isolated from Iraq; and strain MKTC1 (accession number: MT982722.1), which was isolated from India. A new *A. baumannii* strain charmoK was found to belong to a monophyletic clade alongside strains A1(accession numbers: PP659668.1) isolated from China, K70 (accession numbers: KU922251.1) isolated from China, and L50 (accession numbers: KU922297.1) isolated from China. In contrast, a new *S. haemolyticus* strain charmoH was discovered to be related to a monophyletic group beside strains isolate 1 (accession numbers: PP784656.1) isolated from Iran, J12 (accession numbers: KP324951.1) isolated from India, and H-120 (accession numbers: MN595082.1) isolated from India. Similarly, *S. aureus* strain charmoS shares a monophyletic clade with strain IRQBAS78 gene (accession numbers: LC499784.1), previously identified from Iraq.

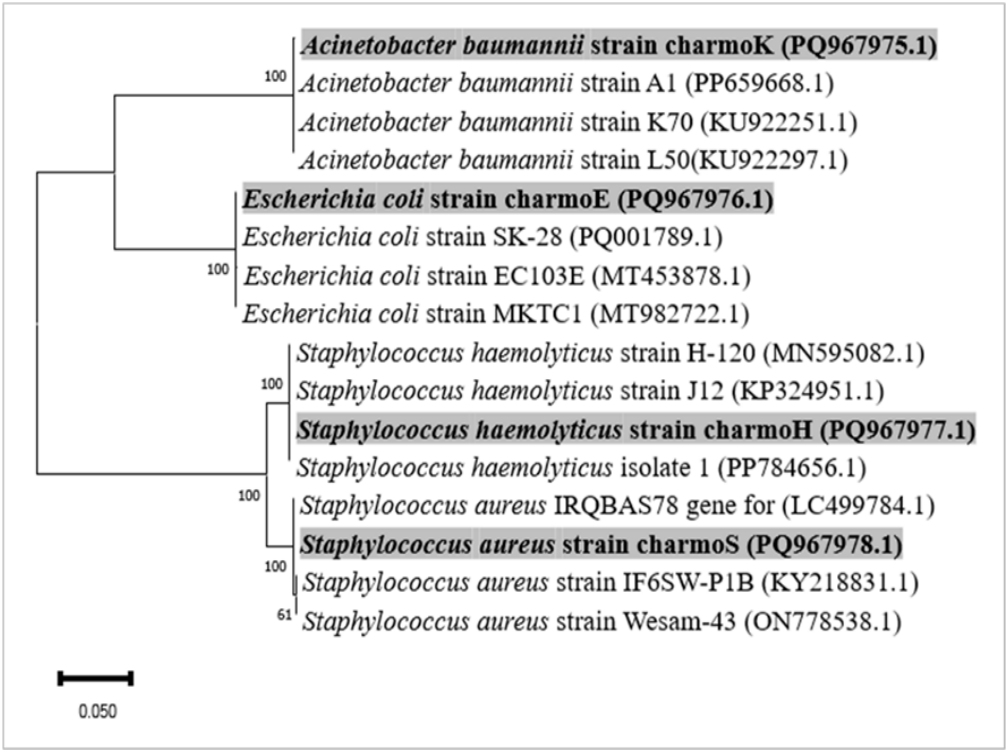

Figure 3. Phylogenetic tree of A. baumannii charmoK, E. coli charmoE, S. haemolyticus charmoH, and S. aureus charmoS using 16S rRNA gene nucleotide sequence similarities. The new isolates in this research are highlighted in bold. The tree is created using the neighbor-joining approach in ClustalX and MEGA 7, bootstrapped with 1000 replicates

3.2. Biosynthesis and Characterization of Ha-AgNPs

The aqueous leaf extract of H. amplifolium served as the reductive and capping agent for Ag^{+} during Ha-AgNP synthesis. This is because the plant extract is known to contain flavonoids, antioxidants, and phenolic components that act as reducing and stabilizing agents during AgNP biosynthesis, while their functional groups (e.g., hydroxyl and carbonyl groups) facilitate nucleation and stabilization of AgNPs (Agustina et al., 2021). Upon adding the plant extract, the color of the AgNO3 solution changed from colorless to light-brown, suggesting that silver-ions (Ag^{+}) were reduced to metallic-silver (Ag^{0}) and indicating that Ha-AgNPs were made during the reduction phase(Figure 4) (Aslam et al., 2021). It has been recorded that the excitation of the Surface Plasmon Band (SPB) by the Ha-AgNP is responsible for the color changes that occur in the solution. To the best of our knowledge, this is the first experimental use of H. amplifolium leaf extract in the synthesis of Ha-AgNPs.

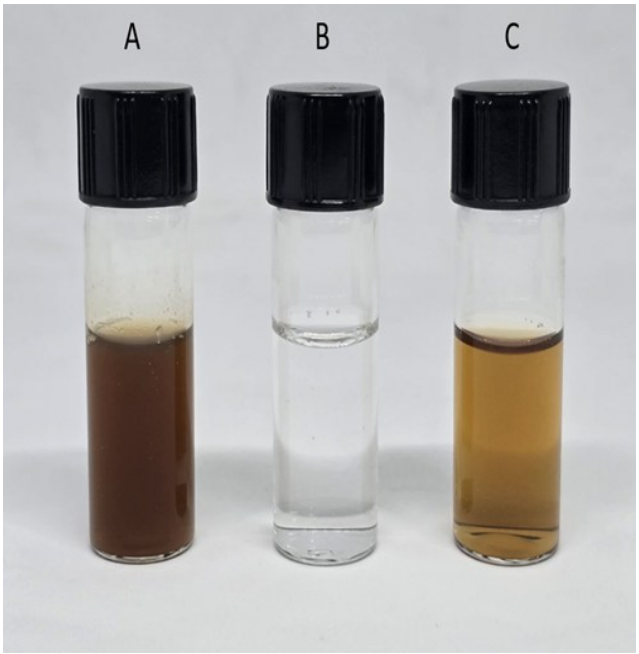

Figure 4. Color change in silver nitrate solution after adding *H. amplifolium* aqueous leaf extract. (A): *H. amplifolium* aqueous leaves extract; (B): Colorless silver nitrate solution; (C): Light brown indicates formation of Ha-AgNPs

Various approaches were used to confirm and characterize the bio-fabricated Ha-AgNPs. Initially, the UV-Vis spectroscopy showed a well-defined SPR peak at around 426 nm (Figure 5), suggesting that Ag^+ ions were reduced by the H. amplifolium leaf extract and formed Ha-AgNPs. The SPR phenomenon is due to the collective oscillation of free electrons on the NPs surface, which results in producing a strong electromagnetic field and a characteristic absorption peak (García, 2011). Previously, a SPR peak at 427 nm has been recorded for AgNPs prepared with Artocarpus heterophyllus leaf extract,(Hudaya et al., 2024), perhaps indicating uniformity of plant associated in the production of AgNP. Additionally, the SPR peak of the biologically produced AgNPs' SPB was detected at 420 nm and 450 nm respectively, using the aqueous extracts of Ocimum gratissimum and Matricaria chamomilla flowers, respectively (Das et al., 2017; Mohamedsalih and Sabir, 2020). Differences in SPR peaks are mainly attributed to variations in size and morphology of nanoparticles and their optical properties (Moores and Goettmann, 2006).

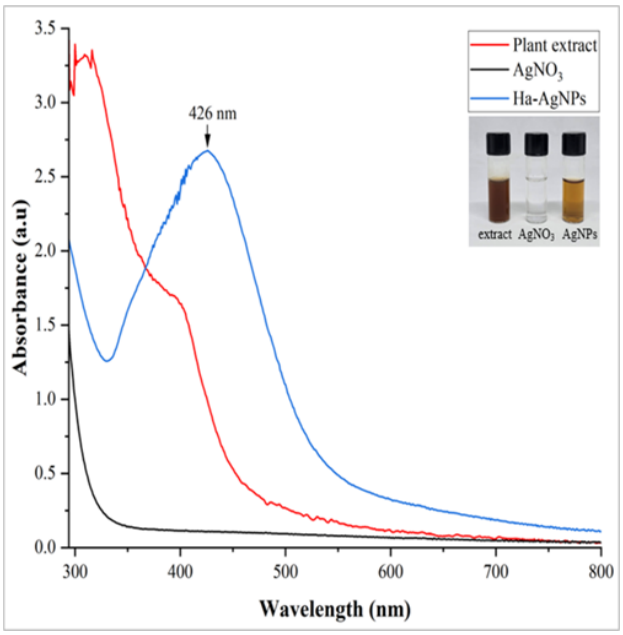

Figure 5. The UV-visible spectrum of Ha-AgNPs produced from plant-extract and $AgNO_3$ solution.

The functional groups in charge of the Ha-AgNP reduction and stabilisation were found using FTIR spectroscopy. The H. amplifolium leaf extract and the Ha-AgNPs spectra were obtained in the region of 4000–500 cm^{-1}. The extract exhibited absorption bands at 3437, 2925, 2854, 1631, 1385, 1107, 617 and 538 cm^{-1} that could be attributed to the functional groups of the plant matrix (Figure 6, red). FTIR of the Ha-AgNPs also showed peaks at 3436, 2925, 2854, 1632, 1456, 1385, 1180, 1112, 775, 618, 471 cm^{-1} (Figure 6, blue) suggesting that the Ag^+ ions were reduced by plant phytochemicals to generate Ag^0 nanoparticles, which were then stabilised and capped during the nanoparticle creation process. Additionally, certain peaks' intensities decreased or increased, and the emergence of other new peaks showed significant shifts. Both plant extract and biosynthesized Ha-AgNPs' wide bands at vibrational around 3437–3436 cm^{-1} is due to O–H and N–H stretching vibrations (Bose and Chatterjee, 2016; Yassin et al., 2022) and indicative of phenolic compounds and flavonoids, which aided in AgNPs synthesis. The peak band near 2925-2854 cm^{-1} was attributed to C-H stretching, which relates to an aliphatic chain (Ramli et al., 2023). The band at about 1632 cm-1 was ascribed to phenolic substances like flavonoids and polyphenols' C=C stretching vibrations (Ramli et al., 2023), and the 1456-1385 cm-1 absorption peak was due to C-N (aromatic amines) and O-H. Whereas those at 1180–1112 cm^{-1} are ascribed to C–OH stretching vibration arising from alcohols or esters, respectively. Peaks around 775–471 cm^{-1}, probably due to Ag–O bond vibrations and polysaccharides related to O–H bending (Hemlata et al., 2020; Diksha et al., 2023). The FTIR spectra of green produced NPs exhibited a modest shift in several associated peaks and their intensities, showing that the key biomolecules from the H. amplifolium extract were capped or bonded to the surface of Ag-O. Peaks seen around and below 700 cm^{-1} may be attributed to metal-ligand vibrations such as Ag-O or probable Ag-N interactions with phytochemicals in the plant extract (Anandalakshmi et al., 2016; Moges and

Misskire, 2025). The peaks at 618 and 471 cm^{-1} verifies binding between Ag atoms and phytoconstituents of the extract. Ghasemi et al. (2024) found peaks at 596 and 494 cm−1 that correlated with AgNPs' attachment to extract functional groups. These findings are consistent with previous studies on biomolecule-mediated AgNP formation, which reported similar peak shifts and spectral features (Aref and Salem, 2020; Ghasemi et al., 2024). Overall, changes in the FTIR spectra indicate the involvement of H. amplifolium leaf metabolites in the reduction and stabilization of Ha-AgNPs.

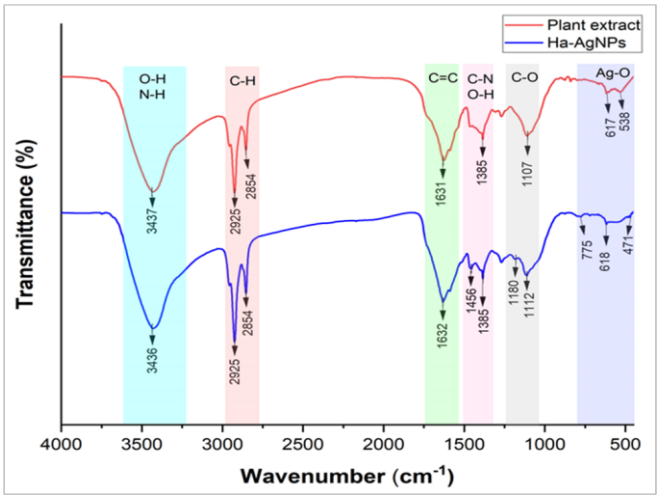

Figure 6. FTIR spectrum of H. amplifolium leaf extract (red) and biosynthetic Ha-AgNPs (blue). The changes in the positions of the absorbance peaks due to phytochemicals interaction with silver ions justify their participation for the nanoparticle reduction and capping.

The crystallinity property and phase of Ha-AgNPs were examined by XRD. XRD investigation was conducted at 2θ in the 10-80° degree range. The Ha-Ag-NPs' XRD pattern, which was produced by reacting an aqueous plant extract of H. amplifolium with a silver salt solution, is presented in (Figure 7). Sharp diffraction peaks, which were located at 2θ angles of 38.32°, 44.53°, 64.71°, and 77.59°, corresponding to the (111), (200), (220), and (311) planes, matching JCPDS card no. 04-0783, consistent with previous findings on plant-mediated extraction, respectively (Meng, 2015; Moges and Misskire, 2025). These results support the formation of crystallized face-centered cubic (fcc) Ha-AgNPs. Slight peak intensity fluctuations in the minor peaks as compared to standard patterns may be attributed to residual phytochemicals derived from leaf extract bound on surface of nanoparticles, which act as capping as well as stabilizing agents. Nevertheless, in contrast to the other peaks, the domain orientation of the peak was discovered in the 38.32° (111) plane, showing a high crystallinity. The stronger planes show that silver plays a significant role in nanoparticle nucleation and growth (Afandy et al., 2023). The mean average crystallite size of prepared Ha-AgNPs was determined to be 19.1 ± 0.1 using the Debye-Scherrer formula. These results are well correlated to that reported by Moges and Misskire (2025), which used Sida schimperiana Hochst. ex A. Rich (Chifrig) leaves extract to biosynthesize AgNPs.

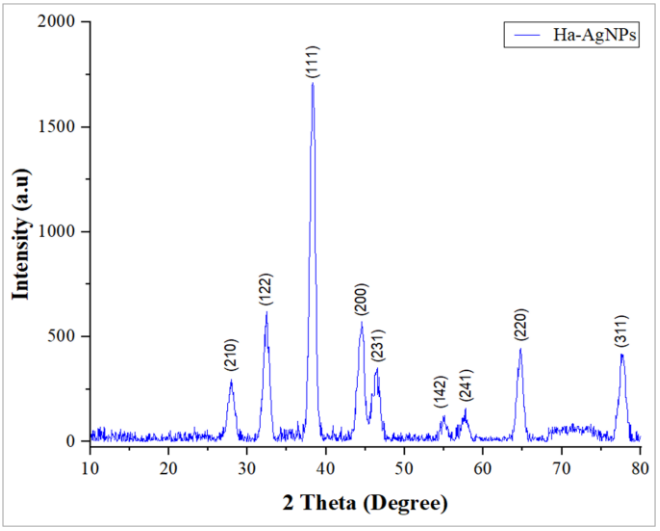

Figure 7. XRD diffraction pattern of biosynthesized Ha-AgNPs created from H. amplifolium leaf extract, verifying their crystalline nature.

The Ha-AgNPs were subjected to morphological analysis using SEM. Prior to analysis, the nanoparticle suspension was dried to obtain solid samples suitable for imaging. The SEM image (Figure 8.a) provided insight into the morphology, size, and surface distribution of the particles that were synthesised. The particles were mainly spherical in shape; however, a degree of size polydispersity was

evident. Some aggregation of nanoparticles was also observed, a common feature of biologically synthesized Ha-AgNPs, likely resulting from their high surface energy, drying-induced interactions, and the variable presence of capping biomolecules on the particle surfaces.

Analysis of individual nanoparticles revealed that the Ha-AgNPs ranged in size from 5 to 50 nm. Measurements from a size-distribution histogram based on 75 single particles by Using ImageJ program, (Figure 8.b) showed a mean particle diameter of 19.93 ± 9.9 nm. Although some degree of aggregation was observed, with clusters reaching sizes of up to ~200 nm, most particles were present as much smaller, discrete nanoparticles. Overall, the average sizes of the Ha-AgNPs are in a good agreement with XRD results and fall within the nanoscale range appropriate for antimicrobial and biomedical applications.

The relatively spherical shaped with size distribution variation, demonstrated in this study, is in agreement with the previously reports on biosynthesized AgNPs. Aslam et al. (2021) and Ghasemi et al. (2024) also have presented that the spherical and polydisperse nanoparticles with an average size of 26 nm and 37 nm, respectively. Additionally, Asimuddin et al. (2020) reported on plant-mediated AgNPs with the size of 20–50 nm, and Raj et al. (2018) described that AgNPs are in size range 20.13 nm, mainly spherical with little aggregation. The nanoparticles in the current study had a relatively small particle size (<20 nm) with a few particles larger than 20 nm, which might give better antimicrobial activity through increased surface area as well as reactivity, whereas mild aggregation as observed will have little impact on overall functional performance.

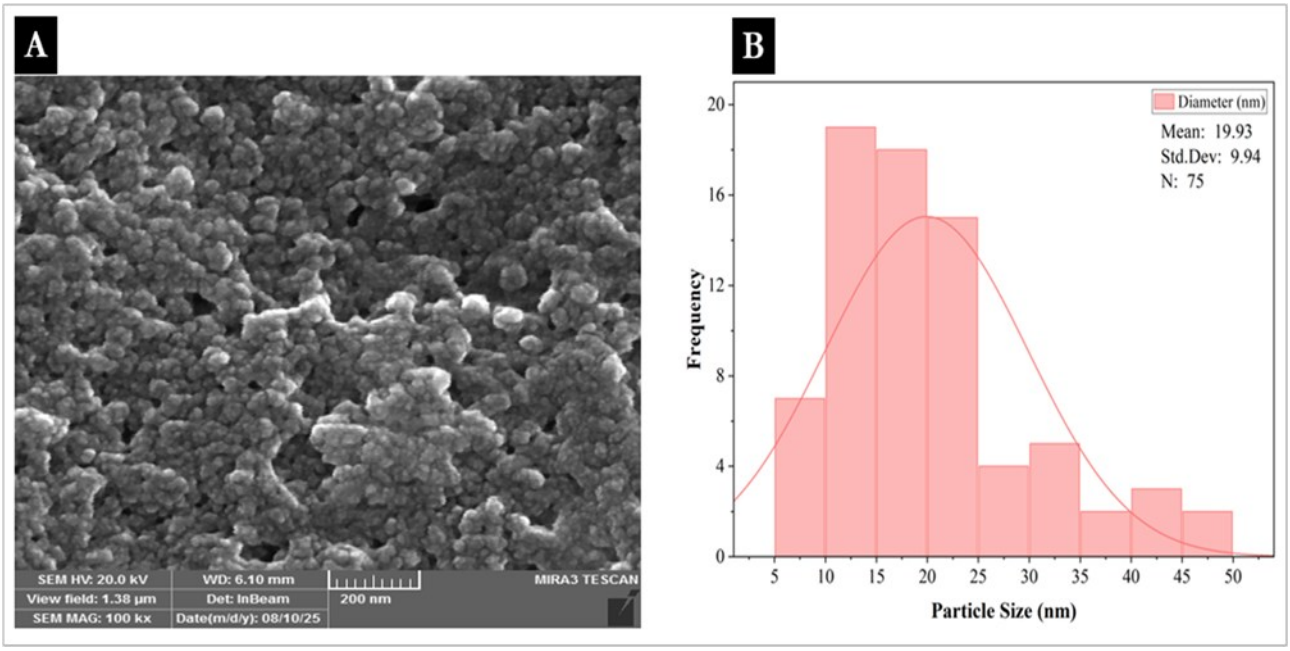

Figure 8. SEM image and size distribution of biosynthesized Ha-AgNPs. (A): SEM image of mostly spherical and polydisperse Ha-AgNPs with slight aggregation. Scale-bar; 200 nm. (B): Size distribution histogram of Ha-AgNPs determined from SEM images (n = 75); the particles were found to be between 5 and 50 nm with an average diameter of 19.93 nm.

The EDS was utilized for analyzing the chemical composition of the biosynthesized Ha-AgNPs (Figure 9). The EDS spectrum displayed a prominent silver peak at approximately 3 keV, corresponding to the Ag Lα line, which confirms the formation of elemental AgNPs (Ghasemi et al., 2024). Silver was the dominant element, accounting for 57.09 wt% and 36.01 at%, indicating successful nanoparticle synthesis.

Minor peaks corresponding to carbon (19.37%), oxygen (13.99%), magnesium (0.16%), phosphorus (1.31%), sulfur (1.90%), chlorine (2.32%), and calcium (3.86%) were also detected (Figure 9). The presence of carbon and oxygen is likely associated with plant-derived phytoconstituents that act as reducing and capping agents during green-synthesis. The carbon-rich signals in the EDS spectra can be attributed to biomolecule substances like vitamins, polyphenols, amino acids, flavonoids, and saponins (Abomuti et al., 2021). Small signals contributions (Mg, P, S, Cl, and Ca) may originate from trace inorganic or organic components of plant-extract.

The comparable results have been observed in other green synthesis of AgNPs; for example, (Yassin et al., 2022) observed a characteristic Ag peak around 3.0 keV in AgNPs biosynthesis using *Origanum majorana* extract. Similarly, AgNPs were biosynthesized using extracts from *Oedera genistifolia* leaves and *Pisum sativum* peels showed dominant silver peaks around 3 keV along with additional signals from plant-based capping molecules (Okaiyeto et al., 2019; Patra et al., 2019). Overall, these results support the effective role of *H. amplifolium* extract as both a reducing and stabilizing agent in silver nanoparticle synthesis.

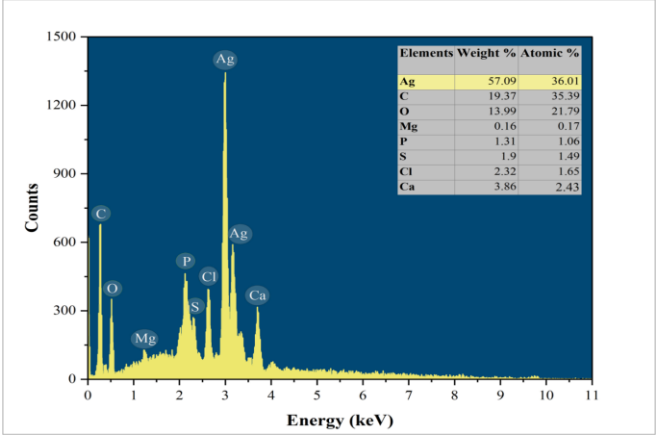

Figure 9. EDS spectrum of biosynthesized Ha-AgNPs. A major prominent Ag peak at around 3 keV confirms the existence of silver nanoparticles, with additional signals (O, Mg, P, S, Cl, and Ca) attributed to phytoconstituent residues originating from H. amplifolium extract, which serve as stabilizing agents.

The HR-TEM was used to investigate morphology and crystalline structure of the biosynthesized Ha-AgNPs. Representative HR-TEM image of biosynthesized Ha-AgNPs is shown in Figure 10.a and Figure 10.c. The nanoparticles were mainly spherical shape, a morphology commonly reported for green-synthesized Ha-AgNPs. A thin, faint layer surrounding the synthesized Ha-AgNPs was visible upon examination, suggesting that the phytoconstituents from the leaf extract served as capping agents, thereby limiting the aggregation of nanoparticles (Some et al., 2019). This observation is consistent with previous green synthesis studies reporting plant-derived capping layers around AgNPs, such as those synthesized using *Phyllanthus emblica* extract (Masum et al., 2019).

The high-resolution image (Figure 10.d) exhibits clear lattice fringes measured by using ImageJ software with the FFT function, confirming the crystalline character of nanoparticles. The measured interplanar spacing of 0.238 nm corresponds to the (111) plane of face-centered cubic (FCC) silver, in good agreement with reported lattice spacings for FCC AgNPs, typically ranging from 0.23 to 0.25 nm (Some et al., 2019; Afandy et al., 2023). Similar FCC lattice structures have been widely reported in plant-mediated formed AgNPs derived from *Rumex hymenosepalus* and *Azadirachta indica*, indicating that plant phytochemicals promote the formation of thermodynamically stable FCC silver nanocrystals (Rodríguez-León et al., 2013; Shahzadi et al., 2025). These finding further support the role of *H. amplifolium* extract not only as a reducing agent but also as an effective capping and stabilizing agent that governs nanoparticle crystallinity and structural quality. In addition, the uniform and continuous lattice fringes demonstrates that Ha-AgNPs are mostly single-crystalline, a feature often associated with high catalytic, optical, and antimicrobial performance (Roy et al., 2014). Overall, these results demonstrate that leaf extract of *H. amplifolium* enables the synthesis of stable, well-defined, and highly crystalline FCC Ha-AgNPs, highlighting its effectiveness in controlling nanoparticle morphology and crystallinity through green synthesis routes.

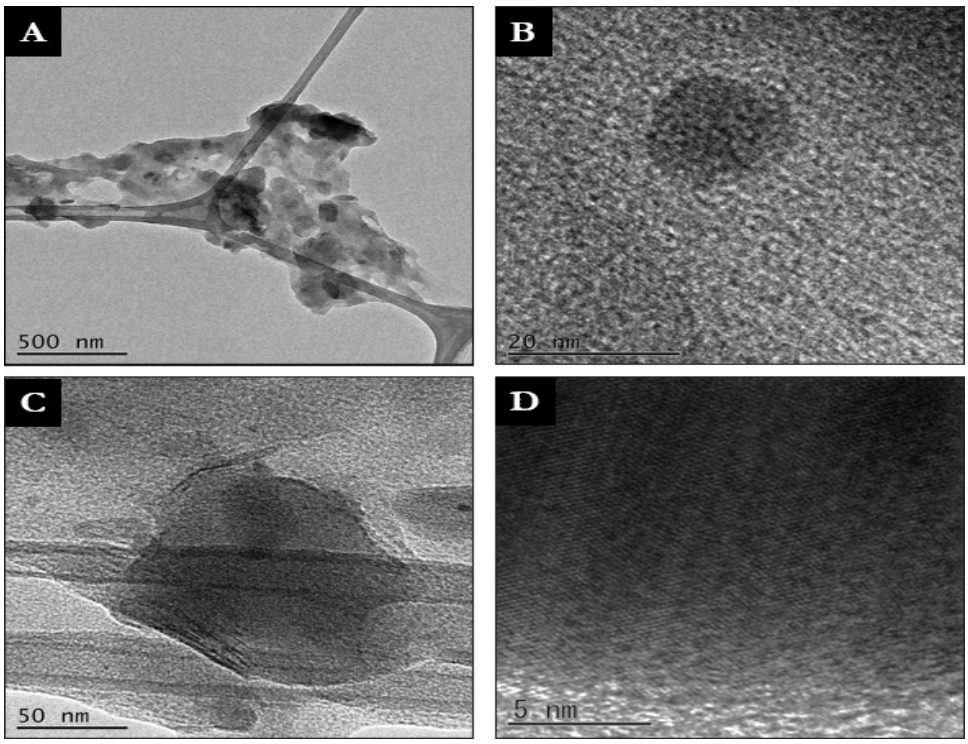

Figure 10. HR-TEM images of Ha-AgNPs obtained with leaf extract of H. amplifolium showing mainly spherical nanoparticles with a thin covering layer (A, C) and distinct lattice fringes corresponding to (111) plane of FCC silver (D).

3.3. Antibacterial Activity Assays of Ha-AgNPs

The antibacterial potential of biosynthesized Ha-AgNPs was tested using MIC and MBC assays. The Ha-AgNPs demonstrated strong antibacterial efficacy against all tested isolates. The concentration range from 6.25 to 100 µg/mL of Ha-AgNPs were tested against the isolates (Figure 11). The lowest MIC (25 µg/mL) and MBC (50 µg/mL) values were recorded for *A. baumannii* strain charmoK. In contrast, *E. coli* strain charmoE, *S. haemolyticus* strain charmoH, and *S. aureus* strain charmoS exhibited MIC values of 50 µg/mL and corresponding MBC values of 75 µg/mL. These findings are consistent with prior studies suggesting that biofabricated AgNPs can have wide-spectrum antibacterial activity, with MIC and MBC values influenced by both nanoparticle properties such as sizes and shapes and the bacterium species (Almatroudi et al., 2020; Ubaid and Alkalifawi, 2022).

As shown in (Figure 11), Ha-AgNPs induced a clear dose-dependent reduction in optical density for all bacterial strains, with maximum inhibition observed at the concentration between 75 and 100 µg/mL. A comparative analysis between Gram negative (*A. baumannii* charmoK, *E. coli* charmoE) and Gram positive (*S. haemolyticus* charmoH, *S. aureus* charmoS) isolates revealed slightly greater inhibition in the Gram-negative bacteria at moderate concentrations (12.5–50 µg/mL). This indicates that AgNPs can penetrate into the thinner peptidoglycan layer and outer membrane of the Gram-negative bacteria more quickly (Shahzadi et al., 2025). At higher concentrations, near-complete growth inhibition was observed in both Gram groups, which could be attributed to strong broad-spectrum activity of Ha-AgNPs.

Variation in susceptibility profiles of the isolates may be attributed to due to the fact that the bacterial samples that were used in this study were clinical samples that were isolated from the local area rather than samples from the ATCC (Said et al., 2024). Multiple mechanisms are proposed to be involved in the antibacterial effects of AgNPs. These mechanisms include the generation of reactive

oxygen species (ROS), disturbance of the structure of bacterial cell membranes, and the internalization of NPs, which results in the blockage of cellular functions (Prabhu and Poulose, 2012; Menichetti et al., 2023). The antibacterial ability of nanomaterials is largely dependent on their physicochemical properties of the nanoparticles including size, shape and surface-area. It has been reported that the smaller particle sizes exhibited better antimicrobial activities compared to the larger counterparts due to bigger specific surface area and enhanced generation of ROS (Dakal et al., 2016; Menichetti et al., 2023). In addition, smaller AgNPs could more efficiently enter inside the bacterial cell and this can contribute to their greater bactericidal action (Dakal et al., 2016).

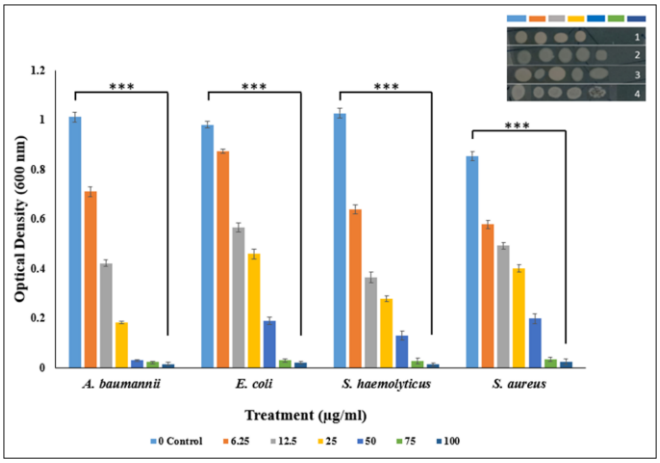

Figure 11. Bacterial isolates were grown in the presence of different concentrations of biologically produced Ha-AgNPs. The mean values from three repetitions of Ha-AgNPs production utilizing H. amplifolium aqueous extract are presented in current data. The accompanying picture validates the MBC values for (1) A. baumannii strain charmoK, (2) E. coli strain charmoE, (3) S. haemolyticus strain charmoH, and (4) S. aureus strain charmoS. Statistical significance was determined by one-way ANOVA (GraphPad Prism), with *** indicating $p < 0.001$ compared with untreated controls.

3.4. Antibiofilm Activity of Ha-AgNPs

Biofilms are a major clinical concern due to their role in antimicrobial resistance and device-associated infections. Accordingly, the antibiofilm efficacy of the *H. amplifolium*–mediated AgNPs was tested against the studied biofilm-forming bacteria: *A. baumannii* strain charmoK, *E. coli* strain charmoE, *S. haemolyticus* strain charmoH and *S. aureus* strain charmoS. Initially, bacterial biofilms were formed in 96-well plates and then exposed to Ha-AgNPs at sub-MIC concentrations of 0.78 to 25 µg/mL. Control wells exhibited dense crystal violet staining, indicative of robust biofilm development, whereas increasing concentrations of Ha-AgNPs progressively resulted in reduced staining intensity (Figure 12). Quantitative analysis demonstrated that Ha-AgNPs exhibited strong antibiofilm activity against all tested Gram positive and negative isolates (Figure 12). *A. baumannii* charmoK showed 97.38% inhibition at 12.5 µg/mL, while maximal inhibition of *E. coli* charmoE (99.17%), *S. haemolyticus* charmoH (99.31%), and *S. aureus* charmoS (98.51%) was achieved at 25 µg/mL. These results are in agreement with previously reported antibiofilm activities of biosynthesized AgNPs, as described by Almatroudi et al. (2020), who recorded potent inhibition activity at 12.5 µg/mL against different Gram positive and negative species. Consistent with these results, Qayyum et al. (2017) reported reduced biofilm formation on AgNP-coated catheters, highlighting the potential of AgNPs as antimicrobial coatings for medical devices to prevent biofilm development. Moreover, our experiment results revealed that the biosynthesized Ha-AgNPs can reduce the bacterial biofilm formation capacities by different bacterial species.

Consistent with their antibacterial activity, Figure 12 shows that Gram negative isolates were slightly more sensitive than Gram positive isolates at lower Ha-AgNP concentrations (0.78–3.125 µg/mL). This difference may be attributed to structural features of the Gram-negative cell envelope, particularly the thinner peptidoglycan layer, which can facilitate nanoparticle interaction and penetration (Kannaujiya et al., 2023; Shahzadi et al., 2025). At 25 µg/mL, the highest concentration tested, Ha-AgNPs exhibited strong antibiofilm activity against all isolates, demonstrating their broad-spectrum efficacy.

The observed antibiofilm effect suggests that Ha-AgNPs are capable of penetrating the biofilm matrix and interfering with its structural stability. Effective

biofilm eradication requires antimicrobial agents to traverse the polysaccharide matrix and access bacterial cells (Ansari et al., 2014; Hamzah et al., 2018). In this context, inhibition of the exopolysaccharide (EPS) production can reduce biofilm structure strength and cellular adhesion. The AgNPs may pass through this matrix and the released Ag^{+} ions are likely to bind to cysteine residues on EPS-associated proteins, thereby disrupting the matrix formation and weakening biofilm integrity (Ansari et al., 2014; Fattah et al., 2026). Similar EPS-mediated pathways have been reported in other plant-derived AgNP (Hudaya et al., 2024), supporting the antibiofilm mode of action observed in this study.

While the strong antibacterial and antibiofilm activities of HA-AgNPs highlight their potential as alternative antimicrobial agents, their possible cytotoxic effects on mammalian cells remain an important consideration for biomedical applications. Previous studies have shown that the toxicity of AgNPs is largely dose-dependent and influenced by particle size, surface chemistry, and exposure duration (Ahamed et al., 2010; Johnston et al., 2010). At controlled concentrations, AgNPs can exert potent antimicrobial effects while maintaining acceptable levels of cytocompatibility in mammalian cell models (Franci et al., 2015). Nevertheless, further in vitro cytotoxicity and in vivo safety studies are required to fully evaluate the biocompatibility and therapeutic potential of these nanoparticles prior to clinical translation (Rai et al., 2009).

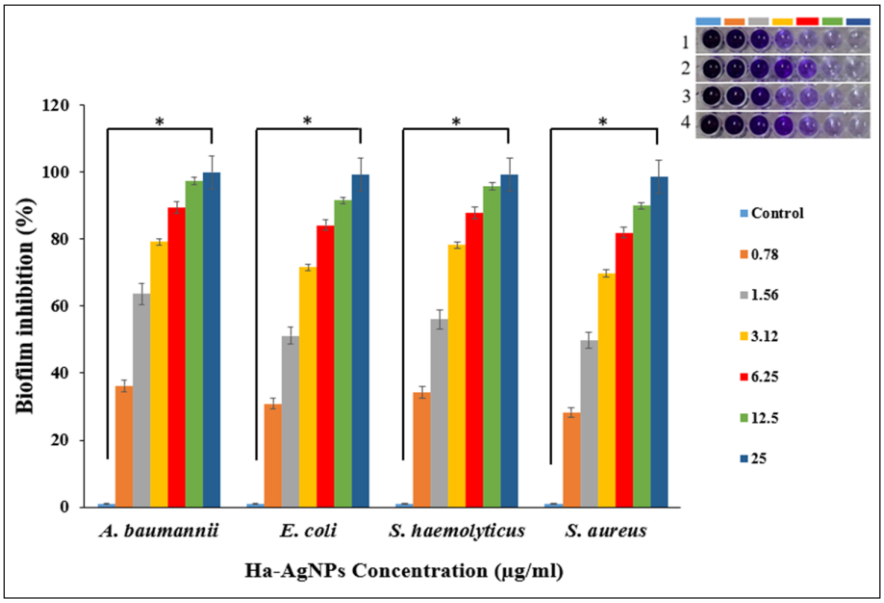

Figure 3. Antibiofilm activity of Ha-AgNPs synthesized from H. amplifolium extract against different bacterial strains at various concentrations. (1): A. baumannii strain charmoK, (2): E. coli strain charmoE, (3): S. haemolyticus strain charmoH, and (4) S. aureus strain charmoS. Statistical significance was assessed using one-way ANOVA (GraphPad Prism), with * indicating $p < 0.05$ compared to untreated controls.

Collectively, the results demonstrate the notable antibiofilm activity of Ha-AgNPs against the tested isolates, highlighting their potential as antimicrobial agents. However, several limitations should be acknowledged. Standard reference strains (e.g., *S. aureus* ATCC 25923 or ATCC 6538) were not included as controls in the antimicrobial assays, which would have enabled more standardized comparisons with previously published studies. In addition, the cytotoxicity and biocompatibility of the synthesized Ha-AgNPs were not evaluated, and therefore further investigations using mammalian cell lines and in vivo models are required to assess their safety, stability, and suitability for biomedical

applications. Moreover, the present study did not investigate the underlying mechanisms responsible for the observed antibacterial and antibiofilm effects. Future studies should therefore explore the mode of action of these nanoparticles through approaches such as membrane integrity analysis, protein leakage assays, DNA damage assessment, and gene expression profiling.

4. Conclusion

This study successfully reports the biofabrication of Ha-AgNPs using aqueous leaf extract of H. amplifolium that can be used to treat pathogenic bacteria causing UTIs. UV-Vis study confirmed the formation of Ha-AgNPs with an absorption peak at 426 nm. Average nanoparticle size was approximately 20 nm, with almost spherical shape as observed by SEM. The biosynthesized Ha-AgNPs have shown a promising antibacterial as well as antibiofilm efficacy against MDR clinical isolates. The Ha-AgNPs also strongly suppressed biofilm formation across all tested pathogens. In general, Ha-AgNPs from H. amplifolium are a promising candidate for alternative antimicrobial agents and should be further explored for applications in therapy.

Conflict of interest

The authors declare no conflict of interest.

Funding

CRediT authorship contribution statement

Acknowledgments

The authors acknowledge the support of Charmo University Research Centre for supplying laboratory equipment and assistance during this investigation. Special thanks go to Assistant Professor Dr. Lanja Hewa Mustafa Khal of the College of Agricultural Herbarium at University of Sulaimani for his kind assistance in identifying and authenticating the plant used in this study.

References

Abadi, A., Rizvanov, A. A., Haertlé, T. & Blatt, N. L., (2019): World Health Organization report: current crisis of antibiotic resistance. BioNanoScience, 9(4), pp.778-788.

Abbasi, R., Shineh, G., Mobaraki, M., Doughty, S. & Tayebi, L., (2023): Structural parameters of nanoparticles affecting their toxicity for biomedical applications: a review. Journal of Nanoparticle Research, 25(3), pp.43.

Abomuti, M. A., Danish, E. Y., Firoz, A., Hasan, N. & Malik, M. A., (2021): Green synthesis of zinc oxide nanoparticles using salvia officinalis leaf extract and their photocatalytic and antifungal activities. Biology, 10(11), pp.1075.

Afandy, H., Sabir, D. K. & Aziz, S. B., (2023): Antibacterial activity of the green synthesized plasmonic silver nanoparticles with crystalline structure against gram-positive and gram-negative bacteria. Nanomaterials, 13(8), pp.1327.

Agustina, T. E., Handayani, W. & Imawan, C. The UV-VIS spectrum analysis from silver nanoparticles synthesized using Diospyros maritima blume. Leaves extract. 3rd KOBI Congress, international and national conferences (kobicinc 2020), 2021. Atlantis Press, 411-419.

Ahamed, M., Alsalhi, M. S. & Siddiqui, M., (2010): Silver nanoparticle applications and human health. Clinica chimica acta, 411(23-24), pp.1841-1848. https://doi.org/10.1016/j.cca.2010.08.016.

Ahmad, S. A. & Askari, A. A., (2015): Ethnobotany of the Hawraman region of Kurdistan Iraq. Harvard papers in botany, 20(1), pp.85-89.

Ahmed, A.-A., Hamzah, H. & Maaroof, M., (2018): Analyzing formation of silver nanoparticles from the filamentous fungus Fusarium oxysporum and their antimicrobial activity. Turkish Journal of

Biology, 42(1), pp.54-62. https://doi.org/10.3906/biy-1710-2.

Aisida, S. O., Ugwu, K., Akpa, P. A., Nwanya, A. C., Nwankwo, U., Botha, S. S., Ejikeme, P. M., et al., (2019): Biosynthesis of silver nanoparticles using bitter leave (Veronica amygdalina) for antibacterial activities. Surfaces and Interfaces, 17(pp.100359.

Al Lawati, H., Blair, B. M. & Larnard, J., (2024): Urinary tract infections: core curriculum 2024. American Journal of Kidney Diseases, 83(1), pp.90-100.

Ali, A. Y., Alani, A.-a. K., Ahmed, B. O. & Hamid, L. L., (2024): Effect of biosynthesized silver nanoparticle size on antibacterial and anti-biofilm activity against pathogenic multi-drug resistant bacteria. OpenNano, 20(pp.100213.

Almatroudi, A., Khadri, H., Azam, M., Rahmani, A. H., Al Khaleefah, F. K., Khateef, R., Ansari, M. A., et al., (2020): Antibacterial, antibiofilm and anticancer activity of biologically synthesized silver nanoparticles using seed extract of Nigella sativa. Processes, 8(4), pp.388.

Anandalakshmi, K., Venugobal, J. & Ramasamy, V., (2016): Characterization of silver nanoparticles by green synthesis method using Pedalium murex leaf extract and their antibacterial activity. Applied Nanoscience, 6(3), pp.399-408.

Ansari, M. A., Khan, H. M., Khan, A. A., Cameotra, S. S. & Pal, R., (2014): Antibiofilm efficacy of silver nanoparticles against biofilm of extended spectrum β-lactamase isolates of Escherichia coli and Klebsiella pneumoniae. Applied Nanoscience, 4(7), pp.859-868.

Aref, M. S. & Salem, S. S., (2020): Bio-callus synthesis of silver nanoparticles, characterization, and antibacterial activities via Cinnamomum camphora callus culture. Biocatalysis and agricultural biotechnology, 27(pp.101689.

Asimuddin, M., Shaik, M. R., Adil, S. F., Siddiqui, M. R. H., Alwarthan, A., Jamil, K. & Khan, M., (2020): Azadirachta indica based biosynthesis of silver nanoparticles and evaluation of their antibacterial and cytotoxic effects. Journal of King Saud University-Science, 32(1), pp.648-656.

Aslam, M., Fozia, F., Gul, A., Ahmad, I., Ullah, R., Bari, A., Mothana, R. A., et al., (2021): Phyto-extract-mediated synthesis of silver nanoparticles using aqueous extract of Sanvitalia procumbens, and characterization, optimization and photocatalytic degradation of azo dyes Orange G and Direct Blue-15. Molecules, 26(20), pp.6144.

Bose, D. & Chatterjee, S., (2016): Biogenic synthesis of silver nanoparticles using guava (Psidium guajava) leaf extract and its antibacterial activity against Pseudomonas aeruginosa. Applied Nanoscience, 6(6), pp.895-901.

Chong, C. S., Sabir, D. K., Lorenz, A., Bontemps, C., Andeer, P., Stahl, D. A., Strand, S. E., et al., (2014): Analysis of the xplAB-containing gene cluster involved in the bacterial degradation of the explosive hexahydro-1, 3, 5-trinitro-1, 3, 5-triazine. Applied and Environmental Microbiology, 80(21), pp.6601-6610.

Dakal, T. C., Kumar, A., Majumdar, R. S. & Yadav, V., (2016): Mechanistic basis of antimicrobial actions of silver nanoparticles. Frontiers in Microbiology, 7(pp.1831.

Das, B., Dash, S. K., Mandal, D., Ghosh, T., Chattopadhyay, S., Tripathy, S., Das, S., et al., (2017): Green synthesized silver nanoparticles destroy multidrug resistant bacteria via reactive oxygen species mediated membrane damage. Arabian Journal of Chemistry, 10(6), pp.862-876.

Diksha, D., Gupta, S. K., Gupta, P., Banerjee, U. C. & Kalita, D., (2023): Antibacterial potential of gold nanoparticles synthesized from leaf extract of Syzygium cumini against multidrug-resistant urinary tract pathogens. Cureus, 15(2), pp.e34830.

Divya, M., Kiran, G. S., Hassan, S. & Selvin, J., (2019): Biogenic synthesis and effect of silver nanoparticles (AgNPs) to combat catheter-

related urinary tract infections. Biocatalysis and agricultural biotechnology, 18(pp.101037.

Faruk, O., Hasan, S. E., Jubayer, A., Akter, K., Al Shiam, S. A., Rahman, K. & Ali, M. Y., (2023): Microbial Isolates from Urinary Tract Infection and their Antibiotic Resistance Pattern in Dhaka city of Bangladesh. Journal of Knowledge Learning and Science Technology ISSN: 2959-6386 (online), 2(3), pp.76-87.

Fattah, B., Hamzah, H. & Arif, H., (2022): Antimicrobial and antibiofilm activity of biosynthesized silver nanoparticles against beta-lactamase-resistant Enterococcus faecalis. Applied Biochemistry and Biotechnology, 194(5), pp.2036-2046. https://doi.org/10.1007/s12010-022-03805-y.

Fattah, B., Hamzah, H. & Arif, H., (2026): Evaluation of the antivirulence and anticancer potential of green-synthesized silver/zinc oxide nanocomposites against methicillin-resistant Staphylococcus aureus and melanoma cells. Discover Nano, 21(1), pp.16. https://doi.org/10.1186/s11671-026-04444-6.

Franci, G., Falanga, A., Galdiero, S., Palomba, L., Rai, M., Morelli, G. & Galdiero, M., (2015): Silver nanoparticles as potential antibacterial agents. Molecules, 20(5), pp.8856-8874. https://doi.org/10.3390/molecules20058856.

García, M. A., (2011): Surface plasmons in metallic nanoparticles: fundamentals and applications. Journal of physics D: applied physics, 44(28), pp.283001.

Ghasemi, S., Dabirian, S., Kariminejad, F., Koohi, D. E., Nemattalab, M., Majidimoghadam, S., Zamani, E., et al., (2024): Process optimization for green synthesis of silver nanoparticles using Rubus discolor leaves extract and its biological activities against multi-drug resistant bacteria and cancer cells. Scientific reports, 14(1), pp.4130.

Hamzah, H. M., Salah, R. F. & Maroof, M. N., (2018): Fusarium mangiferae as new cell factories for producing silver nanoparticles. Journal of microbiology and biotechnology, 28(10), pp.1654-1663. https://doi.org/10.4014/jmb.1806.06023.

Hasan, I., Ozeki, Y. & Kabir, S. R., (2014): Purification of a novel chitin-binding lectin with antimicrobial and antibiofilm activities from a Bangladeshi cultivar of potato (Solanum tuberosum). Indian J Biochem Biophys, 51(2), pp.142-148.

Hemlata, Meena, P. R., Singh, A. P. & Tejavath, K. K., (2020): Biosynthesis of silver nanoparticles using Cucumis prophetarum aqueous leaf extract and their antibacterial and antiproliferative activity against cancer cell lines. ACS omega, 5(10), pp.5520-5528.

Hudaya, I. R., Situmorang, V. C., Hardianto, F. A., Putra, E. D. L., Satria, D., Hertriani, T., Hartati, R., et al., (2024): Biofabrication of silver nanoparticles using Artocarpus heterophyllus leaves extract: Characterization and evaluation of its antibacterial, antibiofilm, and antioxidant activities. Journal of Crystal Growth, 644(pp.127827.

Johnston, H. J., Hutchison, G., Christensen, F. M., Peters, S., Hankin, S. & Stone, V., (2010): A review of the in vivo and in vitro toxicity of silver and gold particulates: particle attributes and biological mechanisms responsible for the observed toxicity. Critical reviews in toxicology, 40(4), pp.328-346. https://doi.org/10.3109/10408440903453074.

Joseph, T. M., Kar Mahapatra, D., Esmaeili, A., Piszczyk, Ł., Hasanin, M. S., Kattali, M., Haponiuk, J., et al., (2023): Nanoparticles: taking a unique position in medicine. Nanomaterials, 13(3), pp.574.

Kalishwaralal, K., Barathmanikanth, S., Pandian, S. R. K., Deepak, V. & Gurunathan, S., (2010): Silver nanoparticles impede the biofilm formation by Pseudomonas aeruginosa and Staphylococcus epidermidis. Colloids and Surfaces B: Biointerfaces, 79(2), pp.340-344.

Kannaujiya, R. M., Chaki, S. H., Khimani, A. J., Giri, R. K., Hirpara, A. B., Vaidya, Y. H. & Deshpande, M. P., (2023): Mechanistic insights into antibacterial and anti-biofilm activities against multidrug-resistant microbes of SnTe nanospheres synthesized by sonochemical method. Chemical Physics Impact, 6(pp.100219.

Kumar, S., Stecher, G. & Tamura, K., (2016): MEGA7: molecular evolutionary genetics analysis version 7.0 for bigger datasets. Molecular biology and evolution, 33(7), pp.1870-1874.

Larkin, M. A., Blackshields, G., Brown, N. P., Chenna, R., Mcgettigan, P. A., Mcwilliam, H., Valentin, F., et al., (2007): Clustal W and Clustal X version 2.0. bioinformatics, 23(21), pp.2947-2948.

Masum, M. M. I., Siddiqa, M. M., Ali, K. A., Zhang, Y., Abdallah, Y., Ibrahim, E., Qiu, W., et al., (2019): Biogenic synthesis of silver nanoparticles using Phyllanthus emblica fruit extract and its inhibitory action against the pathogen Acidovorax oryzae strain RS-2 of rice bacterial brown stripe. Frontiers in Microbiology, 10(pp.820.

Meng, Y., (2015): A sustainable approach to fabricating Ag nanoparticles/PVA hybrid nanofiber and its catalytic activity. Nanomaterials, 5(2), pp.1124-1135.

Menichetti, A., Mavridi-Printezi, A., Mordini, D. & Montalti, M., (2023): Effect of size, shape and surface functionalization on the antibacterial activity of silver nanoparticles. Journal of Functional Biomaterials, 14(5), pp.244.

Moges, W. & Misskire, Y., (2025): Green synthesis, characterization and antibacterial activities of silver nanoparticles using Sida schimperiana Hochst. ex A. Rich (Chifrig) leaves extract. Discover Materials, 5(1), pp.34.

Mohamedsalih, P. M. & Sabir, D. K., (2020): Biosynthesis of silver nanoparticles using the aqueous extract of chamomile flower and their antibacterial activity against Acinetobacter spp. Health Biotechnology and Biopharma, 3(4), pp.48-62.

Mohanta, Y. K., Biswas, K., Jena, S. K., Hashem, A., Abd_Allah, E. F. & Mohanta, T. K., (2020): Anti-biofilm and antibacterial activities of silver nanoparticles synthesized by the reducing activity of phytoconstituents present in the Indian medicinal plants. Frontiers in Microbiology, 11(pp.1143.

Moores, A. & Goettmann, F., (2006): The plasmon band in noble metal nanoparticles: an introduction to theory and applications. New Journal of Chemistry, 30(8), pp.1121-1132.

Nemma, N. M. & Sadeq, Z. S., (2023): Green route of synthesis ag NPs using reductant and stabilizer agent from plants extract as an efficient antibacterial and antifungal activity. Chem. Methodol, 7(pp.325-334.

Okaiyeto, K., Ojemaye, M. O., Hoppe, H., Mabinya, L. V. & Okoh, A. I., (2019): Phytofabrication of silver/silver chloride nanoparticles using aqueous leaf extract of Oedera genistifolia: Characterization and antibacterial potential. Molecules, 24(23), pp.4382.

Pachaiappan, R., Rajendran, S., Show, P. L., Manavalan, K. & Naushad, M., (2021): Metal/metal oxide nanocomposites for bactericidal effect: A review. Chemosphere, 272(pp.128607.

Patra, J. K., Das, G. & Shin, H.-S., (2019): Facile green biosynthesis of silver nanoparticles using Pisum sativum L. outer peel aqueous extract and its antidiabetic, cytotoxicity, antioxidant, and antibacterial activity. International journal of nanomedicine, pp.6679-6690.

Pieroni, A., Ahmed, H. M. & Zahir, H., (2017): The spring has arrived: traditional wild vegetables gathered by Yarsanis (Ahl-e Haqq) and Sunni Muslims in Western Hawraman, SE Kurdistan (Iraq). Acta Societatis Botanicorum Poloniae, 86(1), pp.1-17.

Prabhu, S. & Poulose, E. K., (2012): Silver nanoparticles: mechanism of antimicrobial action, synthesis, medical applications, and toxicity effects. International nano letters, 2(1), pp.32.

Qalatopzany, H., Lazim, Z. & Al-Nashi, T., (2025): Phytochemical and biological studies of Hellenocarum amplifolium grown wildly in Sulaymaniyah, Iraq. Iraqi Journal of Agricultural Sciences, 56(5), pp.1658-1670.

Qayyum, S., Oves, M. & Khan, A. U., (2017): Obliteration of bacterial growth and biofilm through ROS generation by facilely synthesized green silver nanoparticles. PloS one, 12(8), pp.e0181363.

Rai, M., Yadav, A. & Gade, A., (2009): Silver nanoparticles as a new generation of antimicrobials. Biotechnology advances, 27(1), pp.76-83. https://doi.org/10.1016/j.biotechadv.2008.09.002.

Raj, S., Mali, S. C. & Trivedi, R., (2018): Green synthesis and characterization of silver nanoparticles using Enicostemma axillare (Lam.) leaf extract. Biochemical and biophysical research communications, 503(4), pp.2814-2819.

Ramli, N. R., Yusoff, H. M., Maulidiani, M., Asari, A. & Wahab, N. H. A., (2023): Stability of green synthesis of silver nanoparticles by using Euphorbia milii (Euphorbiaceae) leaves extract with different solvents and polarities. Malaysian Journal of Analytical Sciences, 27(4), pp.766-776.

Rodríguez-León, E., Iñiguez-Palomares, R., Navarro, R. E., Herrera-Urbina, R., Tánori, J., Iñiguez-Palomares, C. & Maldonado, A., (2013): Synthesis of silver nanoparticles using reducing agents obtained from natural sources (Rumex hymenosepalus extracts). Nanoscale research letters, 8(1), pp.318.

Roy, K., Sarkar, C. K. & Ghosh, C., (2014): Green synthesis of silver nanoparticles using fruit extract of Malus domestica and study of its antimicrobial activity. Dig. J. Nanomater. Biostruct, 9(3), pp.1137-1147.

Said, A., Abu-Elghait, M., Atta, H. M. & Salem, S. S., (2024): Antibacterial activity of green synthesized silver nanoparticles using Lawsonia inermis against common pathogens from urinary tract infection. Applied Biochemistry and Biotechnology, 196(1), pp.85-98.

Satokari, R. M., Vaughan, E. E., Akkermans, A. D., Saarela, M. & De Vos, W. M., (2001): Bifidobacterial diversity in human feces detected by genus-specific PCR and denaturing gradient gel electrophoresis. Applied and Environmental Microbiology, 67(2), pp.504-513.

Shahzadi, S., Fatima, S., Shafiq, Z. & Janjua, M. R. S. A., (2025): A review on green synthesis of silver nanoparticles (SNPs) using plant extracts: a multifaceted approach in photocatalysis, environmental remediation, and biomedicine. RSC advances, 15(5), pp.3858-3903.

Sher, E. K., Džidić-Krivić, A., Sesar, A., Farhat, E. K., Čeliković, A., Beća-Zećo, M., Pinjic, E., et al., (2024): Current state and novel outlook on prevention and treatment of rising antibiotic resistance in urinary tract infections. Pharmacology & therapeutics, 261(pp.108688.

Shriram, V., Khare, T., Bhagwat, R., Shukla, R. & Kumar, V., (2018): Inhibiting bacterial drug efflux pumps via phyto-therapeutics to combat threatening antimicrobial resistance. Frontiers in Microbiology, 9(pp.2990.

Singh, B. & Agri, H., (2024): A comparative study on antimicrobial susceptibility of uroculturome of humans in health and urinary tract infections. Infect Dis Res, 5(3), pp.11.

Slavin, Y. N., Asnis, J., Häfeli, U. O. & Bach, H., (2017): Metal nanoparticles: understanding the mechanisms behind antibacterial activity. Journal of nanobiotechnology, 15(1), pp.65.

Some, S., Bulut, O., Biswas, K., Kumar, A., Roy, A., Sen, I. K., Mandal, A., et al., (2019): Effect of feed

supplementation with biosynthesized silver nanoparticles using leaf extract of Morus indica L. V1 on Bombyx mori L.(Lepidoptera: Bombycidae). Scientific reports, 9(1), pp.14839.

Swidan, N. S., Hashem, Y. A., Elkhatib, W. F. & Yassien, M. A., (2022): Antibiofilm activity of green synthesized silver nanoparticles against biofilm associated enterococcal urinary pathogens. Scientific reports, 12(1), pp.3869.

Taha, A. B., (2024): Bacterial etiology and antimicrobial resistance pattern of community-acquired urinary tract infection in older adults. Medicine in Microecology, 22(pp.100114.

Timm, M. R., Russell, S. K. & Hultgren, S. J., (2025): Urinary tract infections: pathogenesis, host susceptibility and emerging therapeutics. Nature Reviews Microbiology, 23(2), pp.72-86.

Ubaid, H. N. & Alkalifawi, E. J., (2022): Biofabrication of silver nanoparticles using Eucalyptus camaldulensis leaf extract and its antibacterial activity againsts multidrug resistance. Biochemical & Cellular Archives, 22(1), pp.381-390. https://connectjournals.com/03896.2022.22.381.

Yassin, M. T., Mostafa, A. a.-F., Al-Askar, A. A. & Al-Otibi, F. O., (2022): Facile green synthesis of silver nanoparticles using aqueous leaf extract of Origanum majorana with potential bioactivity against multidrug resistant bacterial strains. Crystals, 12(5), pp.603.

Zakharova, E. A., Kljuykov, E. V., Degtjareva, G. V., Samigullin, T., Ukrainskaya, U. A. & Downie, S. R., (2016): A taxonomic study of the genus Hellenocarum H. Wolff (Umbelliferae-Apioideae) based on morphology, fruit anatomy, and molecular data. Turkish Journal of Botany, 40(2), pp.176-193.